2016

Self-mixing interferometry and its applications

Yanguang Yu
University of Wollongong, yanguang@uow.edu.au

Yuanlong Fan
University of Wollongong, yf555@uowmail.edu.au

Bin Liu
University of Wollongong, bl987@uowmail.edu.au

Publication Details

Y. Yu, Y. Fan & B. Liu, "Self-mixing interferometry and its applications," in Optical Design and Testing VII, 2016, pp. 100210U-1-100210U-13.

Self-mixing interferometry and its applications

Abstract
This paper reviews the self-mixing interference (SMI) in terms of its operation principle, the features of SMI signals and its configuration. SMI refers to a phenomenon that occurs when a small fraction of the light emitted by a laser is backscattered or reflected by an external target and re-enters the laser active cavity, thus leading to the modulation of the laser output power. This is a remarkably universal phenomenon, occurring in lasers regardless of type. A few application examples are presented based on the research work done in our group, including SMI sensing for displacement measurement, material parameters and laser parameters. An SMI with the laser operating at the relaxation oscillation is introduced which has potential for achieving more sensitive sensing.

Publication Details
Y. Yu, Y. Fan & B. Liu, "Self-mixing interferometry and its applications," in Optical Design and Testing VII, 2016, pp. 100210U-1-100210U-13.

Self-mixing interferometry and its applications

Yanguang Yu*[a], Yuanlong Fan[b] and Bin Liu[a]
[a]School of Electrical, Computer and Telecommunications Engineering, University of Wollongong, Northfields Ave, Wollongong, NSW, 2522, Australia
[b]School of Physics, University of Wollongong, Northfields Ave, Wollongong, NSW, 2522, Australia

ABSTRACT

This paper reviews the self-mixing interference (SMI) in terms of its operation principle, the features of SMI signals and its configuration. SMI refers to a phenomenon that occurs when a small fraction of the light emitted by a laser is backscattered or reflected by an external target and re-enters the laser active cavity, thus leading to the modulation of the laser output power. This is a remarkably universal phenomenon, occurring in lasers regardless of type. A few application examples are presented based on the research work done in our group, including SMI sensing for displacement measurement, material parameters and laser parameters. An SMI with the laser operating at the relaxation oscillation is introduced which has potential for achieving more sensitive sensing.

Keywords: self-mixing interferometry, optical feedback, laser diode

1. INTRODUCTION

In recent years, as an emerging and promising non-contact sensing technique, Self Mixing Interferomerty (SMI) has attracted much attention of researchers[1, 2]. The SMI is based on the self-mixing effect that occurs when a small fraction of laser light emitted by the semiconductor laser (SL) is reflected by an external target and re-enters the SL internal cavity. Compared to other traditional interferometric schemes, e.g., Michelson or Mach-Zender, SMI has the following advantages[1]:

- No optical interferometer external to the source is required. This leads to a simple and compact set-up.
- No alignment is needed because the spatial mode that interacts with the cavity mode is filtered out spatially by the laser itself. This means that detection of the diffusive target's movement becomes possible.
- Sensitivity of the scheme is very high (sub-nm sensitivity).

Due to the above advantages, various applications of the SMI has been developed, such as measurements of metrology, laser parameters, and physical quantities[1]. More specifically, these measurements include displacement, vibration, velocity, distance, linewidth, alpha factor, thickness, refraction index, mechanical resonance, and stress/strain hysteresis, etc.

Generally, it is desired that an SMI operates in a stable mode, in which case the shape of SMI signals is characterized by a parameter called Optical Feedback Factor (OFF)[3] C which is associated with external cavity length, linewidth enhancement factor (LEF) of the laser and the amount of light reflected by the target. At weak feedback regime with $0<C<1$, an SMI signal contains sinusoidal-like fringe structure. At moderate feedback regime, which is for $C>1$, an SMI signal shows asymmetric hysteresis and produces sawtooth-like fringe structure. These stable SMI signals can be used for various applications of sensing and instrumentation as mentioned above[1, 2]. However, when the SMI operates in an unstable mode, the SL output power exhibits a high frequency oscillation (close to the relaxation-oscillation (RO) frequency of the laser[5, 6], usually 2-4GHz) with its amplitude modulated by a slow time varying envelop related to the movement of the external target. In this situation, the laser output is referred to as a relaxation-oscillation self-mixing interference (RO-SMI) signal.

In this paper, we aim to provide a comprehensive review of the stable SMI from the view point of its existing model and applications. In this review, it firstly shows that the theoretical model of the SMI can be derived from either the three mirrors model[7] or the Lang and Kobayashi (LK)[8] model, based on which the characteristics of the SMI signal as well as its mechanism are described. Then, the existing SMI based applications on measuring displacement, Young's modulus and LEF are reviewed. Finally, a highly sensitive SMI sensor with the laser operating at the RO is presented.

* yanguang@uow.edu.au; phone +61242218187

2. SMI OPERATING PRINCIPLE AND ITS FEATURES

2.1 Operating principle

Figure 1 presents a schematic diagram of an SMI, which shows that the core components of an SMI only consist of an SL, a photodiode (PD) and a target. The target forms an external cavity for the laser, and when it moves along the light beam, a modulation in the emitted laser power can be detected by the PD packaged at the rear of the SL and then observed. This modulated power is referred to as an SMI signal which carries the information of the motion of the target as well as the SL itself. Usually, the SMI model can be derived from the classical three mirrors model consisting of a Fabry-Perot (FP) type laser[7] with facet reflection coefficients r_1 and r_2, and the target reflection coefficient of r_3, as shown in Fig. 1.

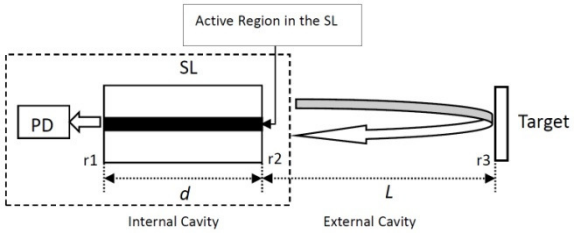

Figure 1. A schematic diagram of an SMI.

Assuming $|r_2 r_3| = 1$, i.e., there is only one reflection within the external cavity, the effective reflection coefficient r_{eff} at the laser front facet can be expressed as[7, 9]:

$$r_{eff} = r_2 + \left(1 - |r_2|^2\right) r_3 e^{-j\omega_s \tau} \tag{1}$$

where ω_s and τ are respectively the perturbed laser angular frequency and one roundtrip time of the light in the external cavity, and $\tau = 2L/c$, where L is the external cavity length and c is the speed of light. On the other hand, r_{eff} can also be represented in another form with respect to its amplitude A_{eff} and phase ϕ_{eff} as [7, 10]:

$$r_{eff} = A_{eff} e^{-j\phi_{eff}} \tag{2}$$

where

$$A_{eff} = r_2 \left[1 + \kappa \cos(\omega_s \tau)\right] \text{ and } \phi_{eff} = \kappa \sin(\omega_s \tau) \tag{3}$$

where κ is the feedback strength and $\kappa = (1 - r_2^2) r_3 / r_2$. As the roundtrip phase in the internal cavity must be equal to a multiple of 2π, the phase condition of compound cavity of the three mirror model can be described using the following equation [7]:

$$\Delta\phi_L = -\alpha(g_c - g_{th})d + \tau_{in}(\omega_s - \omega_0) + \phi_{eff} \tag{4}$$

where $\Delta\phi_L$ corresponds to a change in the round trip phase compared to $2\pi q$, where q is an integer. In Eq. (4), α is called the linewidth enhancement factor (LEF)[4, 11, 12] which is an important fundamental descriptive parameter of the SL because it determines the characteristics of SLs, such as the spectral effects, the modulation response, the injection locking and the response to the external optical feedback[13, 14]. τ_{in} is the light roundtrip time in the internal cavity and ω_0 is the angular frequency of the solitary laser. g_c and g_{th} are respectively the threshold gain with and without external cavity.

$$g_{th} = a_s + d^{-1} \ln\left[(r_1 r_2)^{-1}\right] \tag{5}$$

where a_s represents the loss account for any optical loss in the internal cavity. Note that g_c also must satisfy the amplitude condition of the compound cavity, that is[7, 9, 10]:

$$r_1 A_{eff} e^{\left[(g_c - a_s)d\right]} = 1 \tag{6}$$

Substituting Eqs. (3) and (5) into Eq. (6), we can obtain the threshold gain difference:

$$g_c - g_{th} = -\frac{\kappa}{d}\cos(\omega_s \tau) \tag{7}$$

Then substituting Eqs. (2) and (7) into Eq. (4) and considering $\Delta\phi_L = 0$, equation (4) changes to[7, 9, 10]:

$$\omega_s \tau = \omega_0 \tau - \frac{\kappa}{\tau_{in}} \tau\sqrt{1+\alpha^2}\, \sin\left[\omega_s \tau + \arctan(\alpha)\right] \tag{8}$$

If we denote $\phi_s = \omega_s \tau$, $\phi_0 = \omega_0 \tau$ and $C = \frac{\kappa}{\tau_{in}} \tau\sqrt{1+\alpha^2}$, the core part of the SMI model can be finally derived as:

$$\phi_s = \phi_0 - C\sin\left[\phi_s + \arctan(\alpha)\right] \tag{9}$$

where ϕ_s and ϕ_0 are respectively the light phase corresponding to the perturbed and unperturbed laser angular frequency. Note that although the three mirrors model explains some interesting results, it lacks some details of the physical setting of the phenomenon, e.g., the material and associated effects for an SL[1].

Interestingly, equation (9) can also be derived from the well known Lang and Kobayashi (LK) equations which are based on Lamb's equation and modified with the additional equation for the state concentration[1]. Compared to the three mirrors model, the LK equations describe the active material and carry a description of laser oscillator equations which yield a much more complete description of the dynamic behaviour of a single mode SL with external optical feedback (EOF). The well known LK equations[8] were first proposed in 1980 and the model consists of three simultaneous Delay Differential Equations (DDE) which are shown as below:

$$\frac{dE(t)}{dt} = \frac{1}{2}\left\{G\left[N(t), E(t)\right] - \frac{1}{\tau_p}\right\}E(t) + \frac{\kappa}{\tau_{in}} \cdot E(t-\tau) \cdot \cos\left[\omega_0 \tau + \phi(t) - \phi(t-\tau)\right] \tag{10}$$

$$\frac{d\phi(t)}{dt} = \frac{1}{2}\alpha\left\{G\left[N(t), E(t)\right] - \frac{1}{\tau_p}\right\} - \frac{\kappa}{\tau_{in}} \cdot \frac{E(t-\tau)}{E(t)} \cdot \sin\left[\omega_0 \tau + \phi(t) - \phi(t-\tau)\right] \tag{11}$$

$$\frac{dN(t)}{dt} = \frac{J}{eV} - \frac{N(t)}{\tau_s} - G\left[N(t), E(t)\right]E^2(t) \tag{12}$$

where $G\left[N(t), E(t)\right]$ is the modal gain per unit time and is expressed as[15]:

$$G\left[N(t), E(t)\right] = G_N\left[N(t) - N_0\right]\left[1 - \varepsilon E^2(t)\right] \tag{13}$$

Equations (10)-(13) describe the dynamic behavior of the three variables, namely the electric field amplitude $E(t)$, the electric field phase $\phi(t)$ and the carrier density $N(t)$, where t is the time index. $\phi(t)$ is given by $\phi(t) = \left[\omega(t) - \omega_0\right]t$, and where $\omega(t)$ is the instantaneous optical angular frequency for an SL with EOF.

The dynamics of the SL with an EOF system are governed by the injection current (J) to the SL and the parameters associated with the external cavity including κ and τ. The other parameters in Eqs. (10)-(13) are related to the solitary SL itself, and are treated as constants for a certain SL. These parameters are defined in Table 1[6, 16]. Note that the values of the parameters provided in Table 1 are adopted from[16].

The core part of the SMI model is derived from the stationary solutions of the above LK equations. Let E_s, N_s and ω_s represent the stationary solutions of LK equations for electric field amplitude, carrier density and angular frequency respectively. When the system described by Eqs. (10)-(13) enters into a stationary state, we have $dE(t)/dt = 0$, $d\phi(t)/dt = \omega_s - \omega_0$ and $dN(t)/dt = 0$. Substituting $E(t) = E(t-\tau) = E_s$, $N(t) = N_s$, and $\phi(t) = \left(\omega_s - \omega_0\right)t$ into Eqs. (10)-(13) and ignoring the nonlinear gain, the well known stationary solutions can be obtained as below[8]:

$$\omega_s \tau = \omega_0 \tau - \frac{\kappa}{\tau_{in}} \tau\sqrt{1+\alpha^2}\, \sin(\omega_s \tau + \arctan\alpha) \tag{14}$$

$$N_s = N_0 + \frac{1}{\tau_p G_N} - \frac{2\kappa\cos(\omega_s \tau)}{\tau_{in} G_N} \tag{15}$$

$$E_s^2 = \frac{J/(eV) - N_s/\tau_s}{G_N(N_s - N_0)} \tag{16}$$

Table 1: Physical meanings for the internal cavity parameters in LK equations

Symbol	Physical Meaning	Value
G_N	modal gain coefficient	$8.1\times10^{-13}\,m^3s^{-1}$
N_0	carrier density at transparency	$1.1\times10^{24}\,m^{-3}$
ε	nonlinear gain compression coefficient	$2.5\times10^{-23}\,m^3$
Γ	confinement factor	0.3
τ_p	photon life time	$2.0\times10^{-12}\,s$
τ_{in}	internal cavity round-trip time	$8.0\times10^{-12}\,s$
α	line-width enhancement factor	6.0
e	elementary charge	$1.6\times10^{-19}\,C$
V	volume of the active region	$1.0\times10^{-16}\,m^3$
τ_s	carrier life time	$2.0\times10^{-9}\,s$

From Eqs. (14)-(16) and by considering a moving target, the existing SMI model can be obtained as below by introducing:

$$\phi_0 = \omega_0\tau,\ \phi_s = \omega_s\tau \text{ and } C = \frac{\kappa}{\tau_{in}}\tau\sqrt{1+\alpha^2} \tag{17}$$

Then Eq. (14) becomes the same equation as derived by the three mirrors model (see Eq. (9)), where ϕ_0 is associated with the external cavity length L, i.e., $\phi_0 = 4\pi L/\lambda_0$, where λ_0 is the unperturbed laser wavelength. By substituting Eq. (15) into Eq. (16), the normalized variation of the SL output power (that is the so called SMI signal g) can be obtained and described as[17]:

$$g = \cos(\phi_s) \tag{18}$$

Equations (9) and (18) constitute the existing SMI model which has been widely accepted to describe the waveforms of SMI signals[17]. As seen in Eqs. (9) and (18), there is a straight forward procedure to constitute g, i.e., $\phi_0 \to \phi_s \to g$, and also a straight backward procedure, i.e., $g \to \phi_s \to \phi_0$, to obtain ϕ_0, thus retrieving the external cavity information. Apparently, the knowledge of the theory of generating an SMI signal as well as its waveform is essential to achieve good performance of the SMI.

2.2 Features of SMI signals

SMI signals can be characterized by the value of factor C [3, 18-20] which is an important parameter for SMI systems. The following SMI regimes have been well recognized in literatures:

Regime 1 (weak feedback): where C<1. Equation (9) presents a unique mapping from ϕ_0 and ϕ_s which is shown in Figure 2(a). In this situation, the movement of the external target will result in an SMI signal waveform with a fringe structure similar to a traditional interference fringe, and each fringe period corresponds to a phase shift that is equivalent to a displacement of half a wavelength of the external target[17]. Figure 2 shows the relationship between ϕ_0 and ϕ_s (Fig. 2(a)) as well as g and ϕ_0 (Fig. 2(b)) when $C = 0.7$ and $\alpha = 6$ according to Eqs. (9) and (18). Supposing that the external target moves according to a sinusoidal law with $L(t) = L_0 + \Delta L\cdot\sin(2\pi ft)$, where L_0, ΔL and f are the initial external cavity length the vibration amplitude and frequency respectively which are chosen as $L_0 = 0.35m$, $\Delta L = 1.5\lambda_0$ and $f = 75Hz$, thus leading to a time varying ϕ_0, i.e., $\Delta\phi_0(t) = 4\pi\Delta L(t)/\lambda_0 = 6\pi\cdot\sin(2\pi ft)$ (rad) which is shown in Fig. 2(c), and Fig. 2 (d) shows the corresponding SMI. From Fig. 2(d), it can be seen that, in the weak feedback regime, the SMI signal shows symmetrical sinusoidal fringe shape which is similar to the tradition interference fringes.

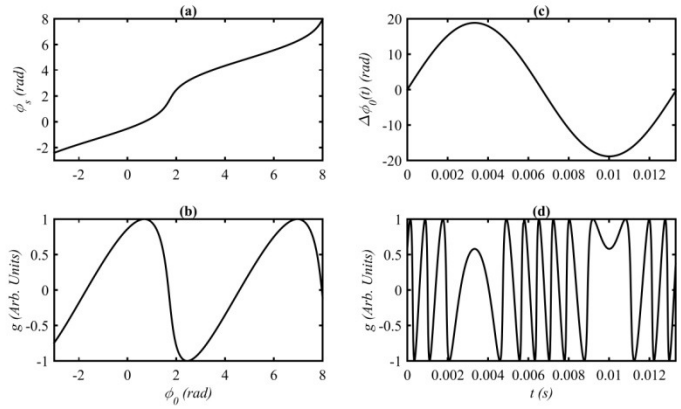

Figure 2: (a) Relationship between ϕ_0 and ϕ_s, (b) relationship between g and ϕ_0, (c) a time varying ϕ_0, i.e., $\Delta\phi_0(t)$, caused by the target movement, (d) corresponding SMI signal when $C = 0.7$ and $\alpha = 6$.

Regime 2 (moderate feedback): where 1<*C*<4.6. In this situation, equation (9) yields three possible ϕ_s. To illustrate the scenario behind the waveform of SMI signal when $1 < C < 4.6$, figure 3 shows the relationship between ϕ_0 and ϕ_s (Fig. 3(a)) as well g and ϕ_0 (Fig. 3(b)) when $C = 3$ and $\alpha = 6$. The actual behaviour is described in[21], indicating that ϕ_s and g will vary along the route $A_1 \rightarrow B \rightarrow B_1$ when ϕ_0 increases, and it will however track the route of $B_1 \rightarrow A \rightarrow A_1$ when ϕ_0 decreases. Note that, the stationary solutions for ϕ_s within the range of $\left[\phi_{s,A}, \phi_{s,B}\right]$ are always unstable according to[21], and thus will never be an oscillating mode of the SMI signal. Similar to the weak feedback regime case discussed above, we present $\Delta\phi_0(t)$, which is same with Fig. 2(c), as well as the corresponding SMI signal g (Fig.3(d)) in the following figure 3. From Fig. 3(d), it can be seen that the SMI signal shows asymmetric hysteresis and produces sawtooth-like fringes. Furthermore, by looking at both Fig. 3 (c) and (d), it can be seen that the slope of each fringe corresponds to the moving direction of the external target, that is a negative slope if the target moves toward the SL, and a positive slope if the target moves away from the SL.

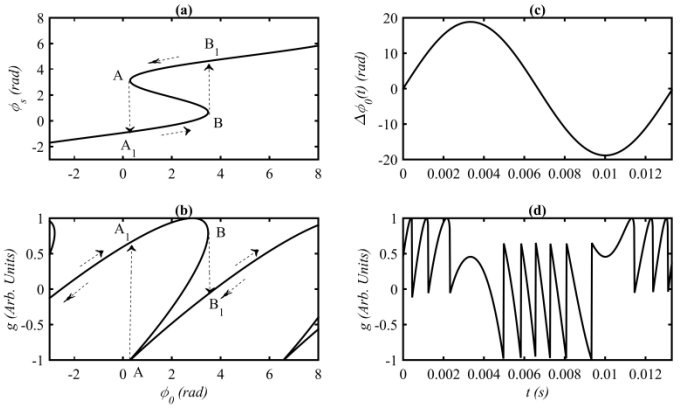

Figure 3: (a) Relationship between ϕ_0 and ϕ_s, (b) relationship between g and ϕ_0, (c) a time varying ϕ_0, i.e., $\Delta\phi_0(t)$, caused by the target movement, (d) corresponding SMI signal when $C = 3$ and $\alpha = 6$.

Regime 3 (strong feedback): where *C*>=4.6. Equation (9) yields seven possible ϕ_s when C=9. Similar to Regime 1 and 2, the scenario behind the waveform of SMI signal when $C > 4.6$ is illustrated in Fig. 4. Figure 4(a) and (b) respectively show the relationship between ϕ_0 and ϕ_s, g and ϕ_0 when $C = 9$ and $\alpha = 6$. This time, ϕ_s and g will vary along the route $B \rightarrow B_1$ when ϕ_0 increases, and it will however track the route of $A \rightarrow A_1$ when ϕ_0 decreases. Note that, the stationary solutions for ϕ_s was selected based on the rule of choosing the one with least minimal linewidth[21]. From

Fig. 4(d), it can be seen that the SMI signal still shows asymmetric hysteresis and produces sawtooth-like fringes which is similar to Fig. 3(d). However, it is interesting to notice that some fringes are lost which is due to strong hysteresis occurred when feedback is strong[21].

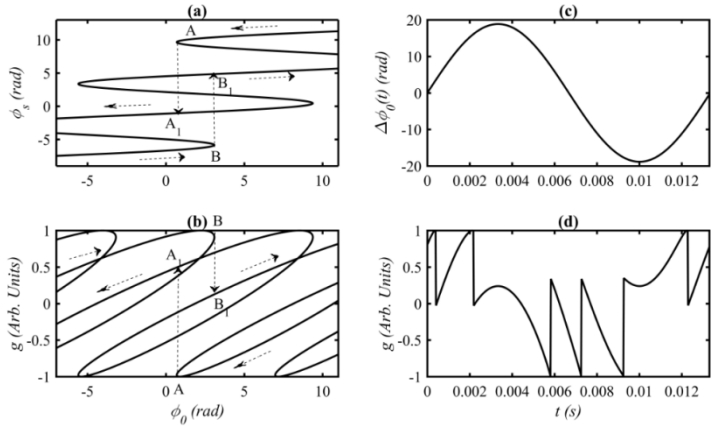

Figure 4: (a) Relationship between ϕ_0 and ϕ_s, (b) relationship between g and ϕ_0, (c) a time varying ϕ_0, i.e., $\Delta\phi_0(t)$, caused by the target movement, (d) corresponding SMI signal when $C = 9$ and $\alpha = 6$.

More information about the mechanism of generating an SMI signal as well as predicting its behaviour with respect to C can be found in[17, 21, 22].

3. SMI BASED APPLICATIONS

3.1 Displacement measurement

Displacement measurement is one of important applications of an SMI-based sensing. Using an SMI to measure displacement can trace its history back to 1995, a fringe counting method[17] is developed based on the fact that each fringe on an SMI signal corresponds to a half-wavelength shift of a moving target. Although the resolution is low (just half-wavelength), this method is simple and the problem of ambiguity in traditional interferometry has been eliminated with the aid of the SMI. In the following decades, various methods, e.g., phase shifting method, phase modulating method, phase unwrapping method *etc.*, are developed with the aim to improve the measurement accuracy. Table 2 summarizes these methods and their corresponding accuracies and restrictions in terms of C.

Table 2: Summary of existing methods for measuring displacement using the SMI.

Methods	Feedback level	Accuracy (resolution)
AM and FM Demodulation Method[23]	Moderate	N/A
Frequency Tuning Method[24]	Weak	10-60 *nm*
Fringe Counting Technique[17]	Moderate	427 *nm* ($\lambda/2$)
Linear Interpolation Method[25]	Weak or Moderate	65 *nm* ($\lambda/12$)
Phase Shifting Method[26]	Weak	65 *nm* ($\lambda/12$)
Speckle Tracking Technique[27]	Moderate	Few part in 10^6 (fraction-of-wavelength)
Fourier Transform Method[28]	Weak	8 *nm* ($\lambda/50$)
Sinusoidal Phase Modulating Method[29]	Weak	Less than 10 *nm* ($\lambda/80$)
Phase Unwrapping Method [14, 30, 31]	Weak or Moderate	Tens of nanometers

Among these methods, the phase unwrapping using advanced signal processing is a very promising technique for SMI based displacement sensing. It is based on the fact that a 2π phase gap corresponds to a fringe on an SMI signal. This technique is more appealing because it does not require any extra optical or electrical elements to be added to the basic SMI sensing structure. Furthermore, this method can achieve higher resolution as it tries to establish a unique mapping from an SMI signal and the laser phase, and the later will give an accurate displacement. The principle of phase unwrapping based displacement measurement can be summarized as following steps:

Step1 Obtain ϕ_s according to Eq. (18) by applying inverse cosine function to g, that is, $\phi_s^r = \arccos(g)$ which is wrapped within the range of $[0, \pi]$.

Step2 Phase unwrap ϕ_s^r in order to obtain the true phase ϕ_s according to:

a. When ϕ_s^r reaches π increasingly, a step of 2π is added to the result of unwrapping operation.

b. When ϕ_s^r reaches 0 decreasingly, a step of 2π should be subtracted to the result of unwrapping operation.

Step3 Calculate ϕ_0 using Eq. (9), and then obtain displacement L using $L = \phi_0 \lambda_0 / (4\pi)$.

Obviously, detection of critical points of an SMI signal is very important as it significantly impacts on the accuracy for estimating ϕ_s and hence the displacement as well.

The phase unwrapping method was first mentioned in 1997[30]. The reconstruction accuracy of this work is in the order of tens of nanometers. Based on[30], Bes *et al.*[31] developed a systematic way to reconstruct displacement under moderate feedback level by introducing an optimization algorithm which jointly estimates C, LEF and the displacement. However, this optimization approach is sensitive to noise contained in an SMI signal because the criterion of optimization depends on the instantaneous power of the reconstructed signal discontinuities[31]. Later, in 2009, based on the work in[31], an improved algorithm is proposed by Zabit *et al.*[32] by introducing the adaptive transition detection, which can automatically converging to the optimal threshold for detecting fringes. In 2011, Fan, *et al.*[14] found that none of the existing phase unwrapping methods is able to perfectly reconstruct displacement from an SMI signal due to an inherent measurement error in these methods. By investigating the features of the fringe shape of an SMI signal in different scenarios, [14] noticed that the error is actually induced due to inaccurate segmentation of each fringe of an SMI signal during the phase unwrapping. For an SMI signal in moderate feedback, its feature can be characterized by four points (marked by *R*, *P*, *V*, and *J* in Fig. 5) and segment of *P* to *J* are ignored by previous methods, thus introducing the errors.

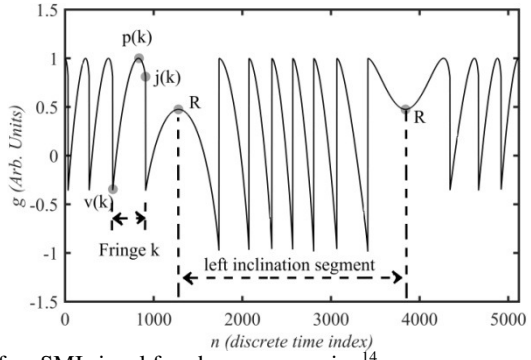

Figure 5: Accurate segmentation of an SMI signal for phase unwrapping[14].

R is called "reverse point," as it is the moment when the target changes its movement direction. *P* and *V* are called the "peak point" and "valley point," respectively, denoting the maximum and minimum points on each fringe. *J* is referred to as the "jumping point," on which an SMI signal exhibits a sudden change. Based these characteristic points, an accurate algorithm is developed based on the following equations:

$$\phi_s(n) = \begin{cases} \phi_s^r(n) + 2\pi(k-1), & when \quad v(k) \le n < p(k) \\ -\phi_s^r(n) + 2\pi(k-1), & when \quad p(k) \le n < j(k) \end{cases} \quad \text{for right-inclined part} \qquad (19)$$

$$\phi_s(n) = \begin{cases} \phi_s^r(n) - 2\pi(K-k+1), & when \quad v(k) \le n < p(k)+1 \\ -\phi_s^r(n) - 2\pi(K-k+1), & when \quad p(k)+1 \le n < j(k) \end{cases} \quad \text{for left-inclined part} \qquad (20)$$

where k is the fringe number. $k = 1, 2, ..., K$ where K is the total fringe numbers in each half segment of an SMI signal. The proposed algorithm in[14] is verified by both simulations and experiments and the results show that the accuracy is improved in contrast to existing techniques.

3.2 Material parameter--Young's modulus

Young's modulus is one of fundamental mechanical parameters for describing various kinds of materials' behaviour, such as porosity, texture and intergranular phases[33]. Therefore, it is of significant interest to know the value of this

parameter since knowledge of Young's modulus is required both for analysis and design. Significant amount of methods have been devoted to determining Young's modulus experimentally[34-37]. However, these methods usually need a dedicated test setup and might not be feasible to carry out in a time and cost effective way. Because of the ease of specimen preparation and a variety of test specimen shapes, SMI based impulse excitation approach[38] is a contactless optical technique, and is experimentally approved with high accuracy and repeatability than traditional methods.

As Young's modulus (denoted by Y) affects the vibration behaviour of material structures, by applying the reverse of this idea, the vibration behaviour of a specific specimen can provide the materials' Young's modulus information. Impulse excitation method is one kind of this technique based on resonant frequency (denoted by f_{RO}) measurement in terms of longitudinal or flexural vibration of the test specimen with simple geometry[39]. For a rectangular specimen (L: length, b: width, h: thickness, m: mass), according to the standard released by ASTM E187621, the calculation formula of Y is expressed as below while $L/h \geq 20$:

$$Y = 0.9465 \cdot \frac{m f_{RO}^2 L^3}{b h^3} \cdot \left[1 + 6.585(h/L)^2\right] \tag{21}$$

Figure 6 shows the fiber-coupled SMI system for capturing the vibration signal $y(t)$ from the test specimen and obtaining f_{RO} [38]. The system mainly consists of a laser diode (LD), coupling fiber and the tested specimen. The LD is at DC biased with the LD controller. The temperature controller is used to stabilize the temperature of the LD. The emitting laser from the LD is focused onto the left end of specimen. A small portion of the light will be back-scattered or reflected by the specimen and re-enter the LD internal cavity. Both the amplitude and frequency of the LD power are modulated by the movement of the specimen. This modulated LD power (denoted by g) is referred to as an SMI signal which is detected by the PD packaged in the rear of the LD and amplified by a trans-impedance amplifier, then recorded by an oscilloscope or collected by personal computer via analog–digital data acquisition (DAQ) card. Figure 7(a) shows an SMI signal obtained via experiment when the specimen is an aluminum alloy 6061 with L=132.43mm, b= 12.24mm, h= 2.00mm and m= 8.70g. The resonant frequency of the specimen is shown in Fig. 7(b) which is 599Hz, thus giving Young's modulus of Y=70.0GPa according to Eq. (21).

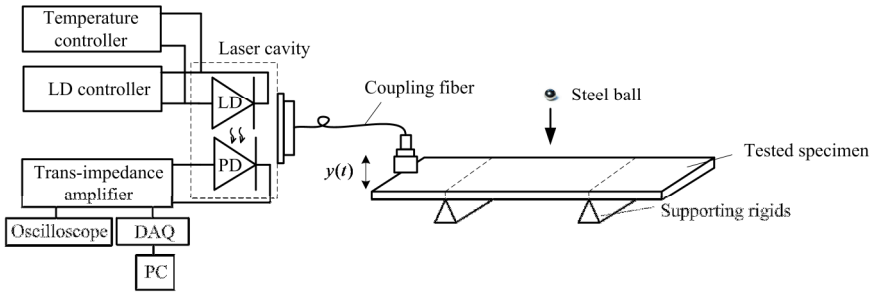

Figure 6: Schematic diagram of fiber-coupled SMI for measuring Young's modulus[38].

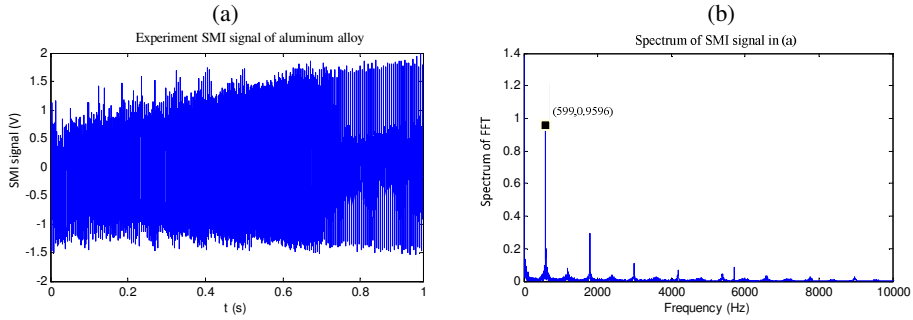

Figure 7: Experimental results for measuring Young's modulus when the specimen is an aluminum alloy[38].

3.3 alpha measurement

The linewidth enhancement factor (LEF) (also referred to as the alpha factor, the α parameter, Henry factor, the chirp factor, or the phase-amplitude coupling factor) is one of fundamental parameters for semiconductor lasers (SLs). The parameter was introduced by Henry in 1982[4]. Its value is very important for describing many aspects of laser behaviour, such as spectral effects, modulation response, injection locking and the response to external optical feedback[12]. Therefore, it is of significant interest to know the value of this parameter since knowledge of alpha is required both for analysis and design. Various methods have been developed for experimental determination of the alpha parameter, which can be categorized as linewidth measurement method, current modulations method, optical injection and optical feedback[12, 40]. Among these methods, the optical feedback method, i.e., the SMI, is an emerging and promising technique which does not require high radio frequency or optical spectrum measurements, thus providing ease of implementation and simplicity in the system structure [1, 13].

In 2004, Yu *et al.*[13] firstly propose the LEF can be obtained using SMI by geometrically measuring the SMI signals' waveform, and this approach requires the characteristic points of the SMI signal, i.e., zero crossing points, to perform the measurement, which means C falls within a small range, i.e., $1 < C < 3.5$. Figure 8 shows a typical experimental SMI signal, where A and B are zero crossing points.

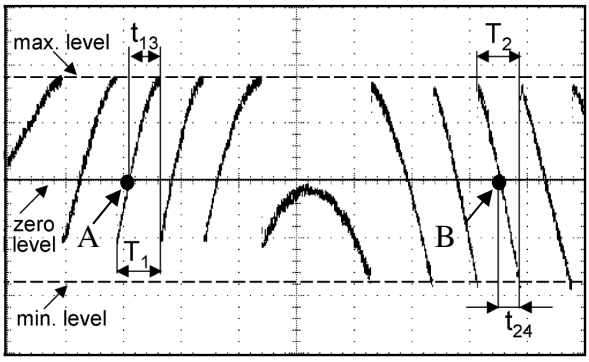

Figure 8: An experimental SMI signal obtained in[13] (see Fig. 2 in[13]) under moderate feedback. Time interval t_{13} and t_{24} are relevant for the determination of α.

The time intervals t_{13} and t_{24} shown in Fig. 7 allow us to determine the phase difference, and thus obtain the value of α based on the following two equations:

$$\phi_{13} = \sqrt{C^2 - 1} + \frac{C}{\sqrt{1+\alpha^2}} + \arccos(-\frac{1}{C}) - \arctan(\alpha) + \frac{\pi}{2} \tag{22}$$

$$\phi_{24} = \sqrt{C^2 - 1} - \frac{C}{\sqrt{1+\alpha^2}} + \arccos(-\frac{1}{C}) + \arctan(\alpha) - \frac{\pi}{2} \tag{23}$$

where $\phi_{13} = 2\pi \frac{t_{13}}{T_1}$ and $\phi_{24} = 2\pi \frac{t_{24}}{T_2}$.

As the above method is limited to the moderate feedback only, in fact, it can just work when 1<C<3, a method in[41] was presented to perform Fourier Transform on an SMI signal to calculate α. The approach in[41] eliminates the feedback level restrictions used in the previous method and provides a fast and easy measurement technique for the LEF.

4. SMI WITH THE LASER OPERATING AT THE RELAXATION OSCILLATION

It is shown in Section 2.1 that the existing mathematical model of the SMI can be derived from steady-state solution of the LK equations[8]. Therefore, the model is valid under the assumption that both electric field $E(t)$ and carrier density $N(t)$ in an SL with a stationary external cavity can reach a constant state after a transient period. However, the work in[5, 16, 42] shows that the relaxation oscillation (RO) or chaos may occur for an SL under certain operation conditions. In this

case, $E(t)$ and $N(t)$ exhibit complicated oscillations rather than a constant level. Depending on the value of C, a recent work in[43] shows that three operational regions (referred to as stable, semi-stable and unstable which are shown in Fig. 9(a)) can be used to describe the behaviour of an SMI. The stable region is where the existing SMI operates. The unstable region is where laser exhibits unstable output and hence not suitable for SMI sensing. It is interesting to note that when an SL operates in the semi-stable region, the waveform of the laser intensity $E^2(t)$ exhibits a stable oscillation and thus is capable of sensing the movement of the external target. By solving the L-K equations, shown in Eqs. (10)-(12), we get the laser intensity $E^2(t)$ (this is SMI signal) and the results are shown in Fig. 9(c)-(g). The parameters' values used for simulation are shown in Table 1.

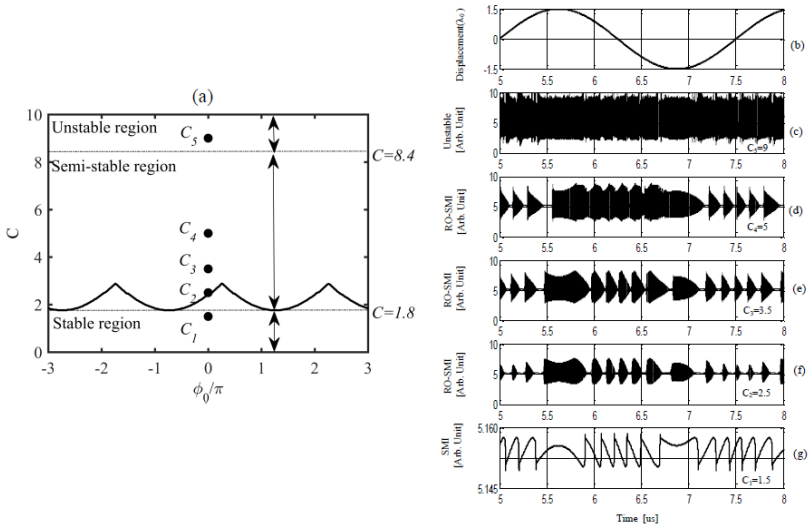

Figure 9: (a) Three operational regions describing the behaviour of an SMI. (b) the target displacement, (c)-(g) the SMI signals corresponding to different C values shown in (a).

Three operational regions can be recognized from the simulation results in Fig. 9, and the features of SMI signals at these regions can be summarized as followings:

1. The signals exhibit the form of high frequency oscillation with its amplitude modulated by a slow-varying signal. Interestingly, the slow-varying envelopes are similar to the SMI signal characterized by the same fringe structure.
2. The Peak-Peak (P-P) value of an SMI signal (in Fig. 9(g)) located in the stable region is around 0.012 while the P-P values of the RO-SMI signals in semi-stable region are about 6.64, 5.04 and 4.12 respectively as shown in Fig. 9(d)-(f) . Hence the RO-SMI signals are much stronger (more than 300 times stronger) than that of the usual SMI signal.
3. When the SMI system enters the unstable region shown in Fig. 9(c), the laser output will be unstable. In this case there is not an obvious relationship between the target movement and the laser output, and hence the system is not suitable for such waveform based sensing.

By using an external fast photo-detector to observe such SMI signals, we obtained experimental signals shown in Fig. 10. In the experiments, the laser source is a commercial semiconductor laser (Hitachi, HL8325G), which is a single mode quantum well laser with the emitting wavelength of 830nm and maximum output power (P) of 40mW. We set its initial external cavity to be $14.5cm$ and the injection current $53mA$. The target is a PZT controlled by a signal with an $30.0V$ DC offset super-positioned with a sinusoidal voltage signal ($200Hz$ and $3.9V$ P-P). The corresponding displacement (P-P) generated by the PZT is $2.08\ \mu m$. The attenuator is adjusted to change the feedback level. It can be seen that the peak-peak value of an RO-SMI signal is much higher than that of the SMI signal in Fig. 10(b). The fringe number in an RO-SMI is the same as the one in the SMI signal. Therefore, we confirm that such SMI has a same displacement resolution with usual SMI signals but a larger signal amplitude.

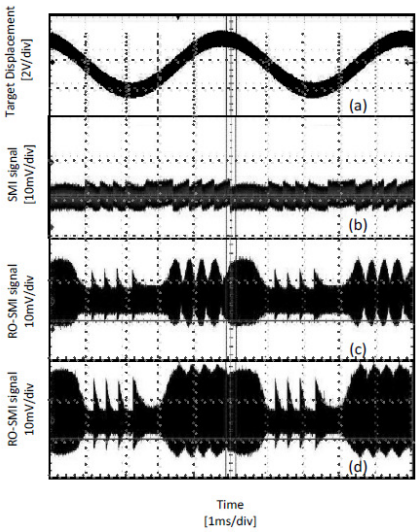

Figure 10: Experimental results of RO-SMI signals.

5. CONCLUSION

This paper presents a thorough overview of the SMI and its applications. Starting from the review of the theoretical background of the SMI, we introduce the operating principle of the SMI, based on which several SMI applications can be developed and are described, including displacement, Young's modulus and alpha measurements. Then, we observe the case when the laser in an SMI operates in relaxation oscillation (RO) from both simulation and experiments. It shows an SMI in such case has potential for achieving more sensitive sensing.

REFERENCES

[1] Donati, S., "Developing self-mixing interferometry for instrumentation and measurements." Laser & Photonics Reviews, 6(3), 393-417 (2012).
[2] Taimre, T., Nikolić, M., Bertling, K., Lim, Y. L., Bosch, T., and Rakić, A. D., "Laser feedback interferometry: a tutorial on the self-mixing effect for coherent sensing." Advances in Optics and Photonics, 7(3), 570-631 (2015).
[3] Acket, G. A., Lenstra, D., Den Boef, A., and Verbeek, B., "The influence of feedback intensity on longitudinal mode properties and optical noise in index-guided semiconductor lasers." IEEE Journal of Quantum Electronics, 20(10), 1163-1169 (1984).
[4] Henry, C., "Theory of the linewidth of semiconductor lasers." IEEE Journal of Quantum Electronics, 18(2), 259-264 (1982).
[5] Tromborg, B., Osmundsen, J., and Olesen, H., "Stability analysis for a semiconductor laser in an external cavity." IEEE Journal of Quantum Electronics, 20(9), 1023-1032 (1984).
[6] Fan, Y., Yu, Y., Xi, J., and Guo, Q., "Stability limit of a semiconductor laser with optical feedback." IEEE Journal of Quantum Electronics, 51(2), 1-9 (2015).
[7] Petermann, K., [Laser diode modulation and noise], Kluwer Academic Publishers ; KTK Scientific Publishers ; Sold and distributed in the U.S.A. and Canada by Kluwer Academic Publishers, Dordrecht ; Boston : Tokyo : Norwell, MA :, (1988).
[8] Lang, R. and Kobayashi, K., "External optical feedback effects on semiconductor injection laser properties." IEEE Journal of Quantum Electronics, 16(3), 347-355 (1980).
[9] Petermann, K., "External optical feedback phenomena in semiconductor lasers." IEEE Journal of Selected Topics in Quantum Electronics, 1(2), 480-489 (1995).
[10] Uchida, A., [Optical communication with chaotic lasers : applications of nonlinear dynamics and synchronization], Wiley-VCH, Weinheim, (2012).
[11] Henning, I. D. and Collins, J. V., "Measurements of the semiconductor laser linewidth broadening factor." Electronics Letters, 19(22), 927-929 (1983).
[12] Osinski, M. and Buus, J., "Linewidth broadening factor in semiconductor lasers--An overview." Journal of Quantum Electronics, 23(1), 9-29 (1987).

[13] Yu, Y., Giuliani, G., and Donati, S., "Measurement of the linewidth enhancement factor of semiconductor lasers based on the optical feedback self-mixing effect." IEEE Photonics Technology Letters, 16(4), 990-992 (2004).
[14] Fan, Y., Yu, Y., Xi, J., and Chicharo, J. F., "Improving the measurement performance for a self-mixing interferometry-based displacement sensing system." Applied Optics, 50(26), 5064-5072 (2011).
[15] Masoller, C., "Implications of how the linewidth enhancement factor is introduced on the Lang and Kobayashi model." IEEE Journal of Quantum Electronics, 33(5), 796-803 (1997).
[16] Mork, J., Tromborg, B., and Mark, J., "Chaos in semiconductor lasers with optical feedback: theory and experiment." IEEE Journal of Quantum Electronics, 28(1), 93-108 (1992).
[17] Donati, S., Giuliani, G., and Merlo, S., "Laser diode feedback interferometer for measurement of displacements without ambiguity." IEEE Journal of Quantum Electronics, 31(1), 113-119 (1995).
[18] Lenstra, D., Van Vaalen, M., and Jaskorzyńska, B., "On the theory of a single-mode laser with weak optical feedback." Physica B+C, 125(2), 255-264 (1984).
[19] Donati, S. and Fathi, M. T., "Transition from short-to-long cavity and from self-mixing to chaos in a delayed optical feedback laser." IEEE Journal of Quantum Electronics, 48(10), 1352-1359 (2012).
[20] Taimre, T. and Raki, A. D., "On the nature of Acket's characteristic parameter C in semiconductor lasers." Applied Optics, 53(5), 1001-1006 (2014).
[21] Yu, Y., Xi, J., Chicharo, J. F., and Bosch, T. M., "Optical feedback self-mixing interferometry with a large feedback factor C: behavior studies." IEEE Journal of Quantum Electronics, 45(7), 840-848 (2009).
[22] Plantier, G., Bes, C., and Bosch, T., "Behavioral model of a self-mixing laser diode sensor." IEEE Journal of Quantum Electronics, 41(9), 1157-1167 (2005).
[23] Donati, S., "Laser interferometry by induced modulation of cavity field." Journal of Applied Physics, 49(2), 495-497 (1978).
[24] Yoshino, T., Nara, M., Mnatzakanian, S., Lee, B. S., and Strand, T. C., "Laser diode feedback interferometry for stabilization and displacement measurements." Applied Optics, 26(5), 892-897 (1987).
[25] Servagent, N., Gouaux, F., and Bosch, T., "Measurements of displacement using the self-mixing interference in a laser diode." Journal of Optics-Nouvelle Revue D Optique, 29(3), 168-173 (1998).
[26] Servagent, N., Bosch, T., and Lescure, M., "Design of a phase-shifting optical feedback interferometer using an electrooptic modulator." IEEE Journal of Selected Topics in Quantum Electronics, 6(5), 798-802 (2000).
[27] Norgia, M., Donati, S., and D'Alessandro, D., "Interferometric measurements of displacement on a diffusing target by a speckle tracking technique." IEEE Journal of Quantum Electronics, 37(6), 800-806 (2001).
[28] Wang, M. and Lai, G. M., "Displacement measurement based on Fourier transform method with external laser cavity modulation." Review of Scientific Instruments, 72(8), 3440-3445 (2001).
[29] Guo, D. M., Wang, M., and Tan, S. Q., "Self-mixing interferometer based on sinusoidal phase modulating technique." Optics Express, 13(5), 1537-1543 (2005).
[30] Merlo, S. and Donati, S., "Reconstruction of displacement waveforms with a single-channel laser-diode feedback interferometer." IEEE Journal of Quantum Electronics, 33(4), 527-531 (1997).
[31] Bes, C., Plantier, G., and Bosch, T., "Displacement measurements using a self-mixing laser diode under moderate feedback." IEEE Transactions on Instrumentation and Measurement, 55(4), 1101-1105 (2006).
[32] Zabit, U., Bosch, T., and Bony, F., "Adaptive transition detection algorithm for a self-mixing displacement sensor." IEEE Sensors Journal, 9(12), 1879-1886 (2009).
[33] Radovic, M., Lara-Curzio, E., and Riester, L., "Comparison of different experimental techniques for determination of elastic properties of solids." Materials Science and Engineering: A, 368(1–2), 56-70 (2004).
[34] Suansuwan, N. and Swain, M., V., "Determination of elastic properties of metal alloys and dental porcelains." Journal of Oral Rehabilitation, 28(2), 133-139 (2001).
[35] Li, C. and Zhu, Z., "Dynamic Young's modulus of open-porosity titanium measured by the electromagnetic acoustic resonance method." Journal of Porous Materials, 13(1), 21-26 (2006).
[36] Salem, J. A. and Singh, A., "Polynomial expressions for estimating elastic constants from the resonance of circular plates." Materials Science and Engineering: A, 422(1–2), 292-297 (2006).
[37] Lord, J. D. and Morrell, R. M., "Elastic modulus measurement—obtaining reliable data from the tensile test." Metrologia, 47(2), S41 (2010).
[38] Lin, K., Yu, Y., Xi, J., Li, H., Guo, Q., Tong, J., and Su, L., "A Fiber-Coupled Self-Mixing Laser Diode for the Measurement of Young's Modulus." Sensors, 16(6), 928 (2016).
[39] Lin, K., Yu, Y., Xi, J., Fan, Y., and Li, H., "Measuring Young's modulus using a self-mixing laser diode," Proc. SPIE, 8975, 89750B-89750B-8 (2014).

[40] Fordell, T. and Lindberg, A. M., "Experiments on the linewidth-enhancement factor of a vertical-cavity surface-emitting Laser." IEEE Journal of Quantum Electronics, 43(1), 6-15 (2007).
[41] Yu, Y. and Xi, J., "Influence of external optical feedback on the alpha factor of semiconductor lasers." Optics Letters, 38(11), 1781-1783 (2013).
[42] Helms, J. and Petermann, K., "A simple analytic expression for the stable operation range of laser diodes with optical feedback." Journal of Quantum Electronics, 26(5), 833-836 (1990).
[43] Fan, Y., Yu, Y., Xi, J., and Guo, Q., "Dynamic stability analysis for a self-mixing interferometry system." Optics Express, 22(23), 29260-29269 (2014).